Versatile bimetallic lanthanide metal-organic frameworks for tunable emission and efficient fluorescence sensing

Su, Yan; Yu, Junhong; Li, Youbing; Phua, Fiona Soo Zeng; Liu, Guofeng; Lim, Wei Qi; Yang, Xiaozhan; Ganguly, Rakesh; Dang, Cuong; Yang, Chaolong; Zhao, Yanli

2018

https://hdl.handle.net/10356/83067

https://doi.org/10.1038/s42004-018-0016-0

Versatile bimetallic lanthanide metal-organic frameworks for tunable emission and efficient fluorescence sensing

Yan Su[1], Junhong Yu[2], Youbing Li[1], Soo Fiona Zeng Phua[3], Guofeng Liu[3], Wei Qi Lim[3], Xiaozhan Yang[1], Rakesh Ganguly [3], Cuong Dang[2], Chaolong Yang[1] & Yanli Zhao [3]

Developing novel lanthanide metal-organic frameworks (Ln-MOFs) to rapidly and reliably differentiate both metal ions in solution and volatile organic compounds (VOCs) in vapor is highly challenging. Here, we describe versatile Eu^{3+}/Tb^{3+}-MOFs based on a flexible ligand. It is noteworthy that the film fabricated using bimetallic $Eu_{0.47}Tb_{0.63}$-MOF and polyvinyl alcohol could serve as an easy and convenient luminescent platform for distinguishing different metal ions and VOCs. The luminescent film exhibits notable fingerprint correlation between the metal ions/VOCs and the emission intensity ratio of Eu^{3+}/Tb^{3+} ions in Ln-MOFs. As a result, the bimetallic Ln-MOFs show fast recognition of Fe^{3+} ion with a response time of <10 s, and can effectively probe styrene vapor within 4 min. Since the developed Ln-MOF film is stable and reliable, this work presents a promising strategy to explore luminescent platforms capable of effectively sensing different metal ions and VOCs.

[1] School of Materials Science and Engineering, Chongqing University of Technology, Chongqing 400054, China. [2] LUMINOUS! Center of Excellence for Semiconductor Lighting and Displays, School of Electrical and Electronic Engineering and The Photonics Institute, Nanyang Technological University, 50 Nanyang Avenue, Singapore 639798, Singapore. [3] Division of Chemistry and Biological Chemistry, School of Physical and Mathematical Sciences, Nanyang Technological University, 21 Nanyang Link, Singapore 637371, Singapore. Correspondence and requests for materials should be addressed to C.D. (email: hcdang@ntu.edu.sg) or to C.Y. (email: yclzjun@163.com) or to Y.Z. (email: zhaoyanli@ntu.edu.sg)

The detection of different metal ions has received great attention due to the increasing content of metal ions in soil and wastewater, which is relevant for environmental and industrial monitoring, human health, food safety, etc[1-4]. Unlike organic contaminants, metal ions cannot be easily biodegraded. More seriously, many heavy metal ions are known to be toxic or carcinogenic[5-8]. Therefore, it is important to develop efficient and economical approaches to sense and distinguish different metal ions. It is well known that iron is ubiquitous in our living environment, and Fe^{3+} cation has extensive applications including playing an important role in biological systems. However, concentrations of Fe^{3+} ions over or below the normal level can seriously affect human health[9-12]. In the past few years, various kinds of analytical methods have been explored for the detection of different metal ions. As compared with other detection approaches, fluorescent sensors possess many advantages, such as high sensitivity, good reliability, and real-time detection[13-17]. While some fluorescent metal-organic frameworks (MOFs) showed a promising potential in probing metal ions[18-22], MOF-based fluorescent platforms for effective and easy detection of different metal ions in aqueous solution have not been well investigated so far.

On the other hand, volatile organic compounds (VOCs) are toxic and harmful substances that are widely present in indoor and outdoor air. These are mainly derived from the emissions of chemical industries, automobile exhausts, building blocks, etc[23, 24]. Therefore, an effective probe of VOCs is another important task for both environment protection and human health. While some porous materials exhibit promising results in sensing VOCs in solution, fluorescence sensing of trace VOCs in vapor is still challenging on account of their low vapor pressure at room temperature[25, 26]. Styrene is a common VOC that is widely used as a precursor for the synthesis of rubber, plastic products, resins, and polyester in synthetic industries[27-29]. As potentially carcinogenic species, styrene vapor can cause harm, such as the irritation of skin, eyes, and respiratory system[30-32]. Among all styrene vapor detection methods reported to date, gas chromatography, surface acoustic wave, and mass spectrometry are most commonly used[33, 34]. However, these techniques are expensive, complicated, bulky, and unportable. Thus, a portable and easy to operate technology is needed. Fluorescence sensing has attracted much attention due to its high sensitivity, low cost, portability, etc. However, fluorescent sensing of styrene with high sensitivity and easy operation has not been well explored so far.

As a promising class of porous materials, lanthanide MOFs (Ln-MOFs) have attracted wide interest for their luminescent properties derived from essential features of lanthanide elements[35-40]. The introduction of suitable organic chromophoric ligands into Ln-MOFs may enhance their light absorption ability to increase the fluorescent emission of Ln^{3+} ions by the so-called "antennae effect"[41]. Therefore, sensing metal ions/VOCs can be realized by tuning the energy transfer efficiency from "antennae" to Ln^{3+} ions through host–guest interactions. A few luminescent Ln-MOFs with optical properties that are responsive to the guest molecules have been developed[42-44]. However, their luminescent signals only respond to specific molecules. Increasing the capability of distinguishing multiple metal ions or organic molecules by luminescent bimetallic Ln-MOFs has not been well investigated.

In this work, we report a series of versatile bimetallic Ln-MOFs, i.e., $[Ln\cdot(CTP\text{-}COOH)(H_2O)_3]$ (Ln-CTP-COOH, Ln = Eu^{3+} and Tb^{3+}), constructed from a flexible ligand hexa-(4-carboxyl-phenoxy)-cyclotriphosphazene (CTP-COOH). These differ from prior literature studies[26, 45], since the characteristic emission intensity of Eu^{3+} (616 nm) and Tb^{3+} (547 nm) ions in bimetallic $Eu_{0.47}Tb_{0.63}$-CTP-COOH highly depends on various guests (metal ions and VOCs). Polyvinyl alcohol (PVA) films containing bimetallic $Eu_{0.47}Tb_{0.63}$-CTP-COOH are fabricated to serve as a convenient platform for selective recognition of different metal ions in aqueous solution and VOCs in vapor. It is notable that the host–guest interactions not only tune the energy transfer efficiency from organic ligand "antenna" to Ln^{3+} ions, but also are able to modulate the energy assignation between Tb^{3+} and Eu^{3+} ($Tb^{3+} \rightarrow Eu^{3+}$) in the Ln-MOFs. The luminescent properties of the Ln-MOFs highly depend on the guest metal ions and VOCs. Therefore, excellent Ln-MOF materials can effectively sense different metal ions and VOCs through two-dimensional (2D) readouts by combining different ratiometric emission intensity of Eu^{3+} and Tb^{3+} ions. As compared with conventional single Ln^{3+} emission intensity-based methods for chemical sensing, the present dual-readout orthogonal identification scheme is expected to be more reliable, accurate, and powerful. More importantly, the Ln-MOFs could achieve recognition of Fe^{3+} ion in aqueous solution with a response time of <10 s and 60% fluorescence quenching, and recognize styrene in vapor within 4 min and 97% quenching efficiency.

Results

Synthesis and structure description. The organic ligand CTP-COOH was prepared in a high yield (94%) using phosphonitrilic chloride trimer and methyl 4-hydroxybenzoate as starting materials (Supplementary Fig. 1), and characterized (Supplementary Figs. 2–6) by Fourier transform infrared (FT-IR) spectroscopy, $^1H/^{13}C$ nuclear magnetic resonance (NMR) spectroscopy, and electrospray ionization mass spectrometry (ESI-MS). Colorless crystals of Ln-CTP-COOH (Ln = Eu and Tb) were successfully synthesized by the solvothermal reaction of ligand CTP-COOH with lanthanide chloride in a mixed solvent of cyclohexanol and deionized water (v/v = 1:1) heated at 100 °C for 5 days. Due to similar coordination behavior of different lanthanide ions, different kinds of Ln^{3+} ions could be introduced into Ln-MOF simultaneously with Ln^{3+} ions distributed randomly over the metal sites. Therefore, seven bimetallic Ln-MOFs, i.e., Eu_xTb_{1-x}-CTP-COOH (x = 0.84, 0.69, 0.47, 0.38, 0.19, 0.12, and 0.06), were prepared by using mixed lanthanide chloride according to above-mentioned method. The contents of Eu^{3+} and Tb^{3+} ions in desired MOFs were determined by inductively coupled plasma mass spectrometry (ICP-MS) and energy-dispersive X-ray (EDX) spectroscopy (Supplementary Table 1 and Supplementary Figs. 7 and 8). The structures of all Ln-MOFs are isostructural to each other, as confirmed by single-crystal X-ray diffraction (Fig. 1 and Supplementary Tables 2 and 3) and FT-IR (Supplementary Fig. 2). The morphology of all Ln-MOFs was studied by field emission scanning electron microscopy (Supplementary Fig. 9). The Ln-MOFs were also characterized by powder X-ray diffraction (XRD) (Supplementary Fig. 10a), and thermogravimetric analysis (TGA, Supplementary Fig. 10b). More importantly, powder XRD curves (Supplementary Fig. 11) and quantum yields (Φ, Supplementary Table 5) of all post-heating Ln-MOFs (150 °C for 10 h) did not show obvious changes as compared with that of pre-heating Ln-MOFs, demonstrating that the structures of all Ln-MOFs in this work were relatively stable. See Supplementary Discussion for further details.

By taking Eu-CTP-COOH as a representative system, Eu-CTP-COOH crystallizes in triclinic space group P-1. The asymmetric unit contains two crystallographic Eu^{3+} ions (Eu1 and Eu2), one independent hexa-carboxylate anion CTP-COO^{6-}, and five coordinated aqua molecules (Fig. 1a). The Eu1 ion is non-coordinated by nine oxygen atoms: seven from four different CTP-COO^{6-} ligands, and two from coordinated water molecules, representing a tri-capped triangular prismatic geometry (Fig. 1b).
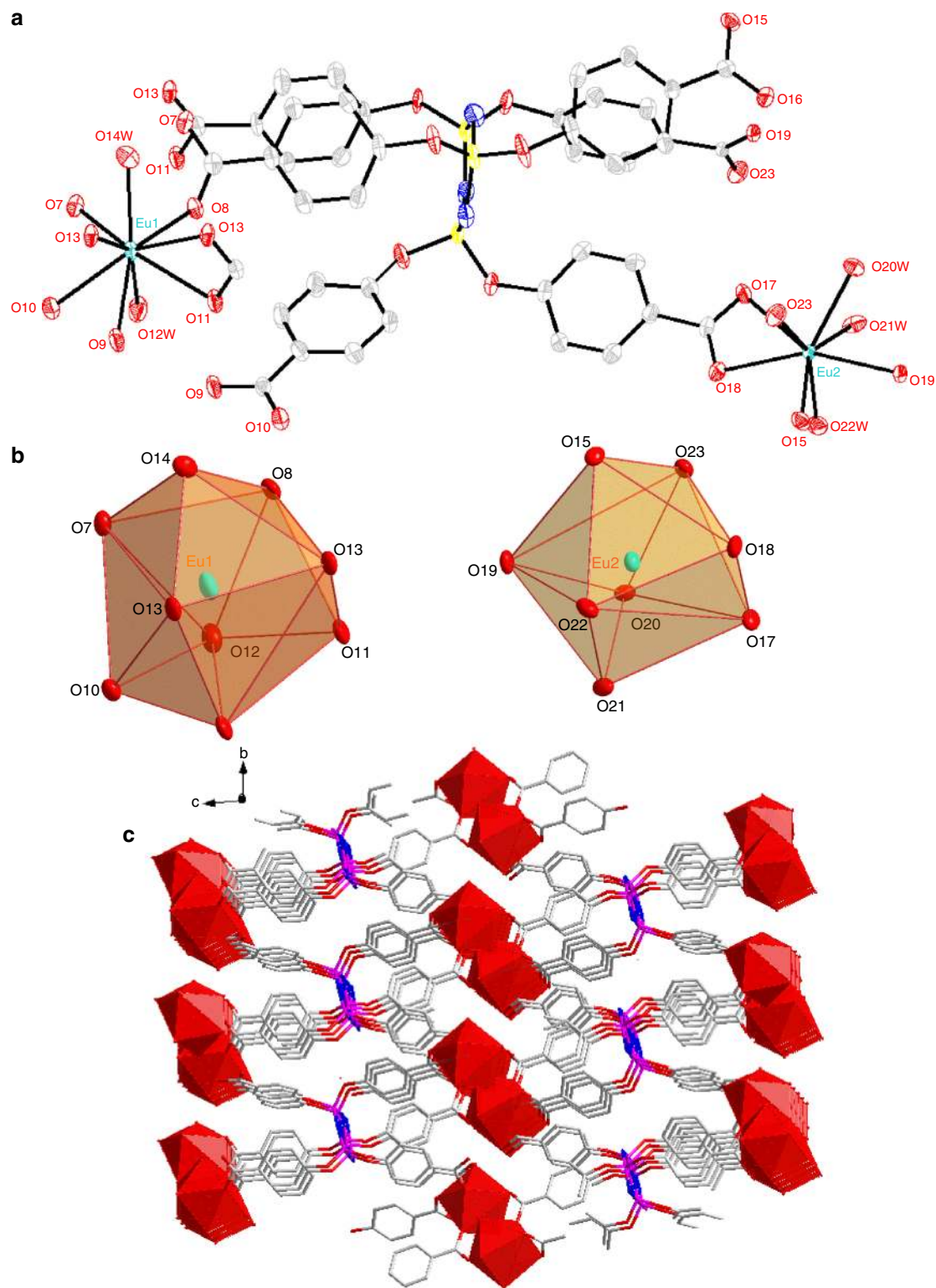
Fig. 1 Crystal structure of Eu-CTP-COOH. **a** Coordination environment around Eu^{3+} ion (50% ellipsoids) with hydrogen atoms being omitted for clarity. **b** Tri-capped triangular prismatic and bi-capped triangular prismatic geometry of Eu1 and Eu2 in Eu-CTP-COOH, respectively. **c** Packing framework of Eu-CTP-COOH, where Eu^{3+} is represented as a polyhedron

The Eu2 ion is coordinated by eight oxygen atoms: five from three different COO^{6-} ligands, and three from coordinated water molecules. The local coordination geometry of the Eu2 ion is bi-capped triangular prismatic (Fig. 1b). The bond length of Eu–O ranges from 2.3238(19) to 2.5932(19) Å, typical values in Eu (III)–carboxylate complexes[46]. Every CTP-COOH^{6-} ligand is

coordinated to eight Eu^{3+} ion centers. The CTP-COOH^{6-} ligand acts as a μ_8-bridge, and four different carboxylate groups adopt μ_2-η^2: η^1, μ_2-η^1: η^1, μ_1-η^1: η^1, and μ_1-η^1:η^0-bridging modes, respectively, (Supplementary Figs. 12 and 13). Eu1 ion and Eu2 ion are connected via four bridging carboxylate acids to form metallic dimers, which are further linked by CTP-COO^{6-} to
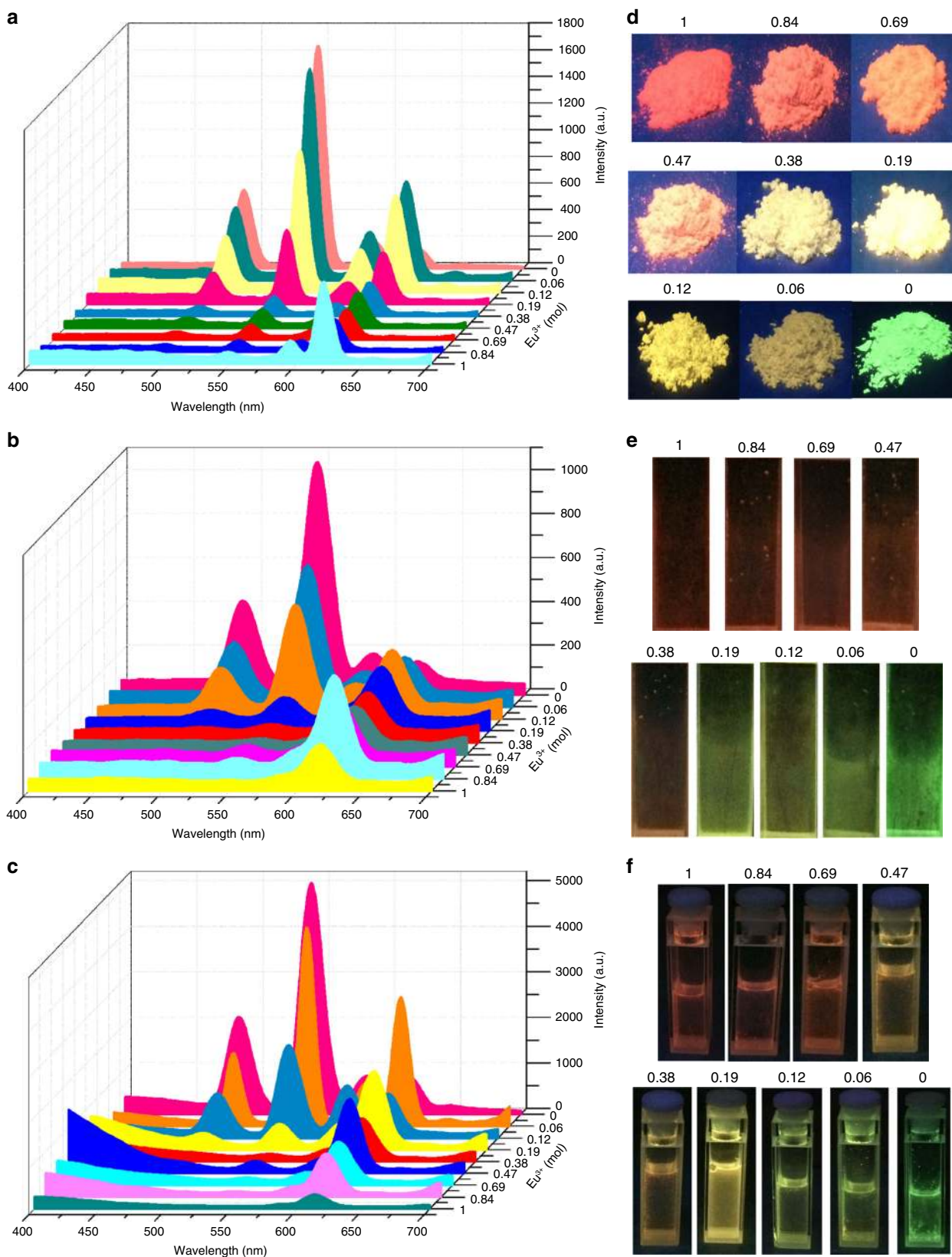
Fig. 2 Emission spectra and corresponding photograph of Ln-MOFs. **a** In powder. **b** In film. **c** In THF solution. **d** Photograph of powder samples under 254 nm UV lamp. **e** Photograph of film samples under 254 nm UV lamp. **f** Photograph of liquid samples under 254 nm UV lamp. Ln-MOFs: Eu_xTb_{1-x}-CTP-COOH ($x = 1$, 0.84, 0.69, 0.47, 0.38, 0.19, 0.12, 0.06, and 0)
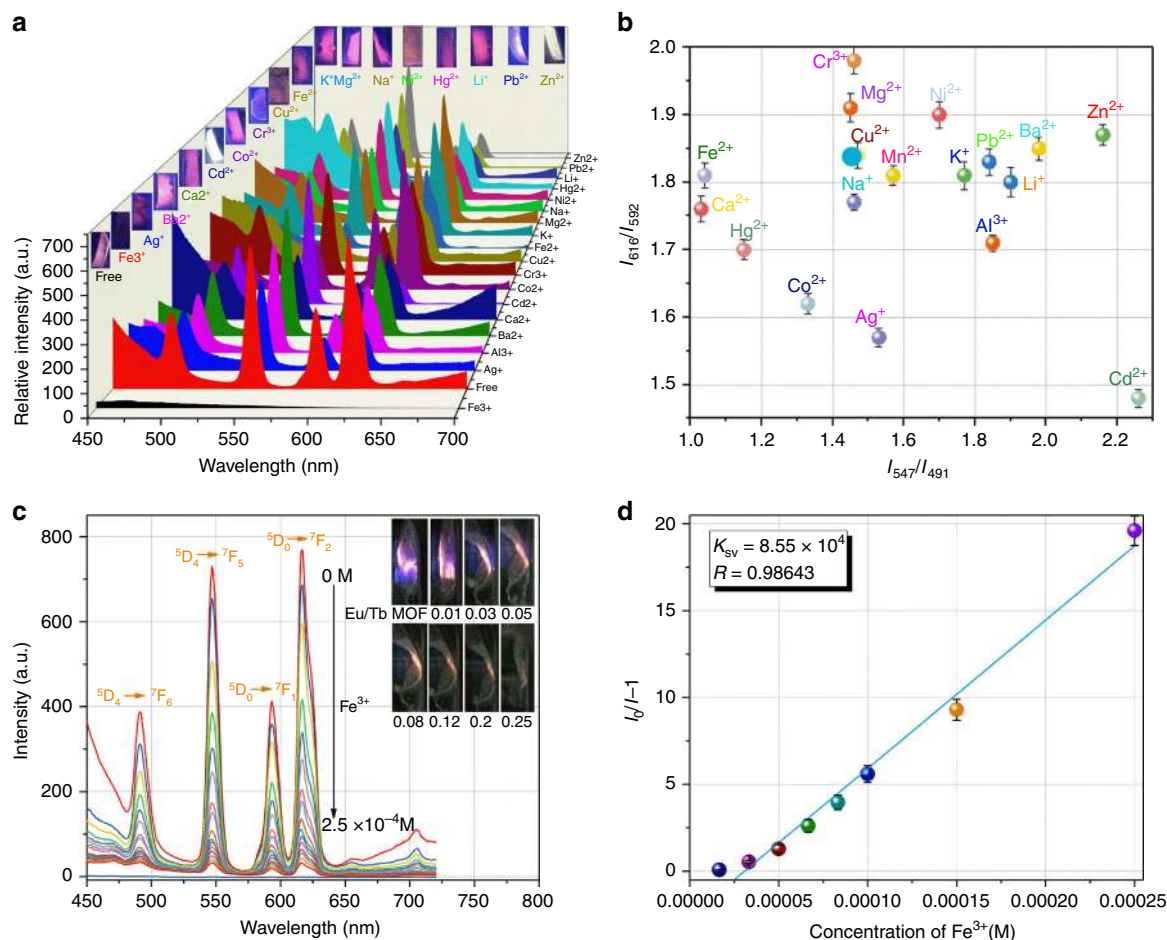
Fig. 3 Metal ion decoding and Fe^{3+} sensing in aqueous solution. **a** Fluorescence response of the $Eu_{0.47}Tb_{0.53}$-CTP-COOH PVA film having different metal ions in aqueous solution with concentration of 1×10^{-2} M for 30 min (λ_{ex}: 280 nm, slit: 5 nm). Inset shows photographs of films having different metal ions under 256 nm UV irradiation. **b** Decoded map for different metal ions based on the ratios of I_{547}/I_{491} and I_{616}/I_{592}. **c** Emission spectra of $Eu_{0.47}Tb_{0.53}$-CTP-COOH PVA film in aqueous solution containing different concentrations of Fe^{3+} ion. Inset shows color changes of $Eu_{0.47}Tb_{0.53}$-CTP-COOH PVA film having different concentrations of Fe^{3+} ion. **d** Stern-Volmer plot of $Eu_{0.47}Tb_{0.53}$-CTP-COOH PVA film quenched by $FeCl_3$ aqueous solution

generate a three-dimensional framework (Fig. 1c). In the crystal structure of Eu-CTP-COOH, the central P_3N_3 ring is nearly planar, the average P–N distance is 1.584 Å, and the average N–P–N and P–N–P angles are 116.38° and 120.98°, respectively. These values are very similar to those of previously reported phosphonitrilic chloride trimer derivatives[47, 48].

Photophysical properties. In powder, film, or THF solution, all Ln-MOFs exhibited characteristic emission with sharp and well-separated emission bands (Fig. 2). The photophysical data of all Ln-MOFs were shown in Supplementary Figs. 14–17 and Supplementary Table 4. In addition, the calculated energy transfer efficiency of the $Tb^{3+} \rightarrow Eu^{3+}$ transition in Eu_xTb_{1-x}-CTP-COOH was over 13% (Supplementary Figs. 18–22), suggesting relatively efficient energy transfer. More importantly, the luminescent colors of these bimetallic Ln-MOFs could be fine-tuned by modulating the ratios of Eu^{3+}/Tb^{3+} during the synthesis procedures (Fig. 2). These luminescent colors also indicate that the organic linker CTP-COOH in MOF structures is an excellent antenna chromosphere to sensitize both Eu^{3+} and Tb^{3+} ions. These samples of Eu_xTb_{1-x}-CTP-COOH ($x = 0.84, 0.69, 0.47, 0.38, 0.19, 0.12, 0.06$) exhibit tunable emission colors controlled through enhancing and weakening the corresponding emission intensities of Eu^{3+} and Tb^{3+} ions under 280 nm irradiation, respectively. The observed emission colors of Eu_xTb_{1-x}-CTP-COOH match

well with the calculated chromaticity coordinates according to the 1931 Commission Internationale deL'Eclairage (CIE) chromaticity diagram. Upon the increase in the ratio of Tb^{3+} in powder, film, and THF solution (Supplementary Fig. 23), the emission colors of these bimetallic Ln-MOFs gradually shift from red region to green region. When the ratio of Eu^{3+} ions is 0.19 ($Eu_{0.19}Tb_{0.81}$-CTP-COOH), near white light emission could be achieved, and the CIE values are (0.37, 0.35) in powder, (0.38, 0.36) in film, and (0.41, 0.34) in THF solution. Especially, a near white light LED was successfully fabricated through coating the phosphor $Eu_{0.19}Tb_{0.81}$-CTP-COOH on the surface of the 280 nm ultraviolet (UV) LED chip. The emission spectrum of white light LED exhibits the characteristic emission of Eu^{3+} and Tb^{3+} ions under a drive voltage of 3 V, and its CIE value is (0.28, 0.30), belonging to near white light (Supplementary Fig. 23d).

Metal ion decoding in aqueous solution. It is understood that single emission intensity of luminescent materials varies on many uncontrollable factors, such as the preparation process of materials, instrument parameters, and concentration of probes[23, 49, 50]. Therefore, the sensing of cations/anions/small molecules through relative emission intensity of luminescent materials is more reliable and accurate than the method using single emission intensity. Because the emission intensity of Eu^{3+} and Tb^{3+} ions in the fluorescent spectrum of $Eu_{0.47}Tb_{0.53}$‾-CTP-COOH excited at 280

nm was comparable, we chose $Eu_{0.47}Tb_{0.53}{-}CTP\text{-}COOH$ as a phosphor to study the sensing properties for different metal ions in aqueous solution. In order to develop a sensor that could be easily reused, a film sensor ($Eu_{0.47}Tb_{0.53}$-CTP-COOH PVA film) was successfully fabricated through doping $Eu_{0.47}Tb_{0.53}$-CTP-COOH into PVA, followed by coating them on the surface of polyethylene glycol terephthalate sheet. As compared with conventional powder sensors based on Ln-MOFs as phosphors[11, 23, 50], the film sensor in this work did not need complicated and time-consuming centrifugal treatment during the cycle experiments. As shown in Fig. 3a, the emission spectra exhibit obvious metal ion-dependent effect: various metal ions induce markedly different effects on the luminescence of $Eu_{0.47}Tb_{0.53}$-CTP-COOH PVA film, particularly for Fe^{3+} ion. The incorporation of Fe^{3+} ion into the $Eu_{0.47}Tb_{0.53}$-CTP-COOH PVA film can drastically quench the characteristic emission of Eu^{3+} and Tb^{3+} ions. However, other metal ions only gave a little (Al^{3+}, Ba^{2+}, Cd^{2+}, Co^{2+}, Cr^{3+}, Fe^{2+}, K^+, Na^+, Ni^{2+}, Li^+, Pb^{2+}, and Zn^{2+}) or mild (Ca^{2+}, Cu^{2+} Mg^{2+}, and Hg^{2+}) effect on the characteristic emission intensity of the $Eu_{0.47}Tb_{0.53}$-CTP-COOH PVA film. Thus, this unique feature could be used for the detection of Fe^{3+} ion in aqueous solution.

It was noted that the film exhibited strong metal ion-dependent luminescence. For example, Cr^{3+}, Ca^{2+}, Na^+, and Ni^{2+} ions gave a significant quenching effect for the emissions of both Eu^{3+} and Tb^{3+} ions, while Mg^{2+}, K^+, Fe^{2+}, Cu^{2+}, and Co^{2+} ions mainly quenched the emission of Tb^{3+} ion, and Ag^+, Al^{3+}, Ba^{2+}, Cd^{2+}, Hg^{2+}, Pb^{2+}, and Zn^{2+} ions showed a quenching effect for the emission of Eu^{3+} ion. These obvious changes in the emission intensity of the Eu^{3+}/Tb^{3+} ions enable the $Eu_{0.47}Tb_{0.53}$-CTP-COOH PVA film to emit metal ion-dependent colors that were clearly distinguishable by the naked eye (inset of Fig. 3a). The above results clearly demonstrate that the metal ions can effectively tune the energy transfer efficiency from "antenna" organic species to Eu^{3+}/Tb^{3+} ions, and also modulate the energy allocation between Eu^{3+} and Tb^{3+} ions in the luminescent spectra of bimetallic Ln-MOFs[11, 50]. Therefore, the tunable energy allocation between Eu^{3+} and Tb^{3+} ions in the luminescent spectra of bimetallic Ln-MOFs could enhance or weaken the emission of Ln^{3+} ion in $Eu_{0.47}Tb_{0.53}$-CTP-COOH PVA film. According to these interesting properties toward different metal ions, a reasonable dual−readout 2D decoded map for different metal ions can be fabricated based on the emission intensity ratios of Tb^{3+} ions (I_{547}/I_{491}) and Eu^{3+} ions (I_{616}/I_{592}) (Fig. 3b). In this decoded map, the information of the metal ions could be obtained by the ratiometric emission intensity of I_{547}/I_{491} and I_{616}/I_{592} from metal ions included $Eu_{0.47}Tb_{0.53}$-CTP-COOH PVA film, i.e., each of the metal ions relates to one unique 2D readout
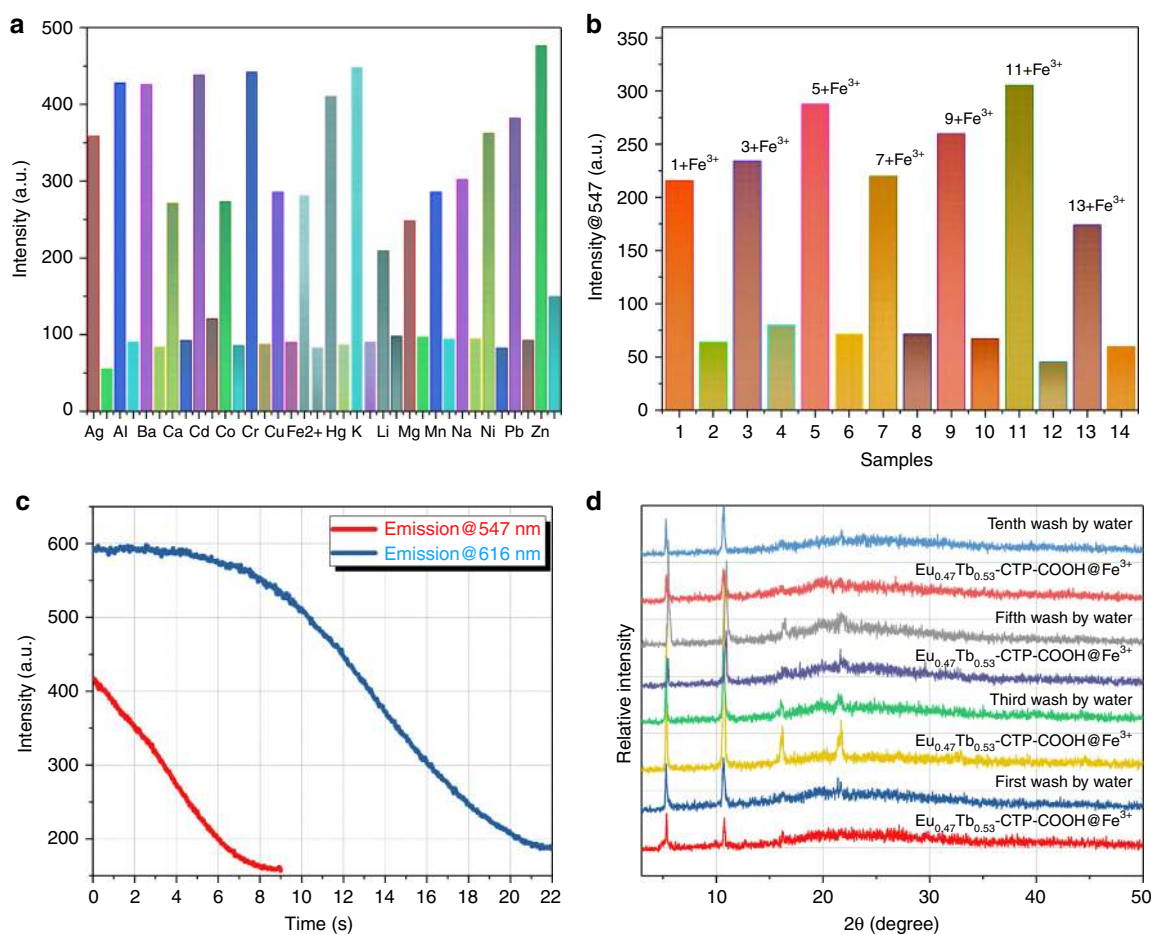

Fig. 4 Anti-interference and reversibility of $Eu_{0.47}Tb_{0.53}$-CTP-COOH PVA film for the detection of Fe^{3+} ion. **a** Competition experiments of the $Eu_{0.47}Tb_{0.53}$-CTP-COOH PVA film for the detection of Fe^{3+} in the presence of other metal ions. **b** Competition experiments for the detection of Fe^{3+} in the presence of five, ten, or more interference metal ions. 1: $Cu^{2+} + Al^{3+} + Co^{2+} + Ba^{2+} + Zn^{2+}$; 2: $1 + Fe^{3+}$; 3: $K^+ + Hg^{2+} + Pb^{2+} + Ca^{2+} + Ni^{2+}$; 4: $3 + Fe^{3+}$; 5: $Li^+ + Ag^+ + Cd^{2+} + Mn^{2+} + Mg^{2+}$; 6: $5 + Fe^{3+}$; 7: $Zn^{2+} + Na^+ + Cr^{3+} + Fe^{2+} + Cu^{2+}$; 8: $7 + Fe^{3+}$; 9: $Cu^{2+} + Fe^{2+} + Al^{3+} + Ni^{2+} + Ca^{2+} + Zn^{2+} + Pb^{2+} + Co^{2+} + Ba^{2+} + Ca^{2+}$; 10: $9 + Fe^{3+}$; 11: $Li^+ + Ag^+ + Cd^{2+} + Mn^{2+} + Mg^{2+} + Zn^{2+} + Na^+ + Cr^{3+} + Hg^{2+} + K^+$; 12: $11 + Fe^{3+}$; 13: all metal ions used except for Fe^{3+}; 14: $13 + Fe^{3+}$. **c** Time-dependent emission intensity of $Eu_{0.47}Tb_{0.53}$-CTP-COOH PVA film incorporated with 1×10^{-4} M Fe^{3+} ion in aqueous solution. **d** Powder XRD patters of $Eu_{0.47}Tb_{0.53}$-CTP-COOH PVA film incorporated with Fe^{3+} ion and washed by deionized water

(I_{547}/I_{491}, I_{616}/I_{592}) in this decoded map. Thus, different metal ions in aqueous solution could be easily recognized and differentiated from this decoded map.

For example, we randomly selected one among these analyte metal ions for the encapsulation into the $Eu_{0.47}Tb_{0.53}$-CTP-COOH PVA film, and obtained the coordinate value of (I_{547}/I_{491}, I_{616}/I_{592}) as (2.16, 1.87). The metal ion could then be recognized as Zn^{2+} ion according to its location in the decoded map. In order to study the influence of counterions on the coordinate values (I_{547}/I_{491}, I_{616}/I_{592}) of metal ions in different metal salts, the coordinate values (I_{547}/I_{491}, I_{616}/I_{592}) of Zn^{2+} ions in $ZnCl_2$, $Zn(NO_3)_2$ and $Zn(CH_3COO)_2$ in aqueous solution were measured, and they are (2.16, 1.87), (2.34, 1.90) and (2.24, 1.82), respectively. As shown in Supplementary Fig. 24, these coordination values of Zn^{2+} ions with different counterions are relatively close in this decoded map, and the exclusive area of Zn^{2+} ion has no overlap with other metal ions' areas.

Detection of Fe^{3+} ion in aqueous solution. To confirm the high sensitivity of the $Eu_{0.47}Tb_{0.53}$-CTP-COOH PVA film for the detection of Fe^{3+} ion, we measured the fluorescence responses of $Eu_{0.47}Tb_{0.53}$-CTP-COOH PVA film in the presence of different concentrations of Fe^{3+} ion. The characteristic emission intensity of the $Eu_{0.47}Tb_{0.53}$-CTP-COOH PVA film gradually decreased upon increasing Fe^{3+} concentration from 0 to 2.5×10^{-4} M, and was completely quenched after the addition of 2.5×10^{-4} M (Fig. 3c). The luminescent colors of the test film samples changed from light red to gray when soaked in different concentrations of $FeCl_3$ aqueous solution. To the naked eye, we can easily distinguish different colors in different Fe^{3+} ion concentrations. Furthermore, the response rate of emission intensity at 547 and 616 nm were also studied. As shown in Fig. 4c, the time-dependent emission intensity of the $Eu_{0.47}Tb_{0.53}$-CTP-COOH PVA film at 547 and at 616 nm was rapidly reduced as soon as 1×10^{-4} M of Fe^{3+} aqueous solution was incorporated, and 60% fluorescence quenching at 547 nm was observed within 10 s and 69% fluorescence quenching at 616 nm within 25 s. These results implied that the response of this film sensor for Fe^{3+} ion is much quicker than that some reported MOFs for Fe^{3+} ion sensing, which could range from minutes to hour[51, 52]. In order to utilize the Ln-MOFs practically, competition experiments were carried out to evaluate the selective ability of $Eu_{0.47}Tb_{0.53}$-CTP-COOH PVA film for the recognition of Fe^{3+} ion through recording its emission intensity in the presence of one, five, ten, or more interference metal ions. As shown in Fig. 4a, b, in the presence of one, five, ten, or more interference metal ions, the $Eu_{0.47}Tb_{0.53}$-CTP-COOH PVA film still showed excellent recognition and sensing properties for Fe^{3+} in aqueous solution.

To further assess the quenching ability of Fe^{3+} ion in aqueous solution, the quenching constant (K_{SV}) was calculated using the Stern-Volmer (SV) equation: $I_0/I = 1 + K_{SV}$ [C]. The I_0 and I are the luminescent intensity at 547 nm in the absence and presence of Fe^{3+} ions, and [C] is the concentration of Fe^{3+} ion. The Stern-Volmer plot for the Fe^{3+} ion showed a good linear correlation, and the value of K_{SV} was estimated to be 8.55×10^4 M^{-1}, revealing a strong quenching effect on the luminescence of $Eu_{0.47}Tb_{0.53}$-CTP-COOH PVA film (Fig. 3d)[53]. In addition, the limitation of detection (LOD) of the film sensor for Fe^{3+} is 3.86 µM (Supplementary Fig. 25). According to the reported results, the LOD of many MOFs for the Fe^{3+} ion ranges from 10^{-3} to 10^{-6} M, meaning that the present film sensor possesses highly sensitive properties for the Fe^{3+} ion in aqueous solution[54]. To examine the recyclability of the film for the Fe^{3+} ion sensing, the film sample was washed with deionized water for 3–5 times after the Fe^{3+} detection, and then the luminescent intensity was

recorded again (Supplementary Fig. 26). The characteristic emission of Eu^{3+} and Tb^{3+} ions can be effectively recovered. Although the emission intensity gradually reduced upon the recycling, the $Eu_{0.47}Tb_{0.53}$-CTP-COOH PVA film can still be used for more than ten times. Facile reusability of the $Eu_{0.47}Tb_{0.53}$-CTP-COOH PVA film could be further certified by powder XRD patterns of the film sensor that was incorporated with Fe^{3+} and washed with water (Fig. 4d). In addition, the common anion NO_3^- exhibited a slight effect on the Fe^{3+} detection (Supplementary Figs. 27 and 28), excluding the disturbance from counterions. Therefore, all above-mentioned results confirm that the $Eu_{0.47}Tb_{0.53}$-CTP-COOH PVA film as a fluorescent probe has high sensitivity and very quick response time for the Fe^{3+} ion detection in aqueous solution. In addition, control experiment results (Supplementary Discussion; Supplementary Figs. 29 and 30) demonstrate that the influence of counterions (such as NO_3^- and Cl^-) on the sensing of Fe^{3+} was not obvious, and Fe^{3+} ion plays a key role for enabling luminescence changes of the $Eu_{0.47}Tb_{0.53}$-CTP-COOH PVA film in aqueous solution even when there was a small number of colloids in the $Fe(NO_3)_3$ and $FeCl_3$ aqueous solution.

Recognition mechanism of Fe^{3+} ion. The underlying mechanism of luminescent quenching by Fe^{3+} ion might be due to following three aspects. The first, the powder XRD pattern of the $Eu_{0.47}Tb_{0.53}$-CTP-COOH PVA film after incorporating Fe^{3+} ion was consistent with that of the as-prepared sample, and thus the collapse of the framework structure could be ruled out (Fig. 4d). The second, very fast response time and recoverable ability indicate that the luminescent quenching cannot be ascribed to the cations exchange, which were further confirmed by the powder XRD (Supplementary Fig. 31). The powder XRD peaks of the $Eu_{0.47}Tb_{0.53}$-CTP-COOH PVA film incorporated with different metal ions have no obvious changes as compared with the original one, indicating that the framework of the Ln-MOFs was not changed during the sensing process. The last, the competitive energy absorption between Fe^{3+} ion and organic ligand CTP-COOH was another possible reason for this phenomenon[55, 56]. There might be a competitive energy absorption process between ligand CTP-COOH and Fe^{3+} ion in aqueous solution when the excitation spectra between the donor and receptor have a certain degree of overlap. Thus, the UV–visible (Vis) spectra of Fe^{3+} ion and other tested metal ions were examined, and the corresponding spectra are shown in Supplementary Fig. 32. The obvious spectral overlap between the absorption spectrum of Fe^{3+} ion and the excitation spectrum of $Eu_{0.47}Tb_{0.53}$-CTP-COOH was observed, suggesting that the excited energy can be effectively absorbed by Fe^{3+} ion to decrease the energy transfer efficiency from ligand CTP-COOH to the Eu^{3+}/Tb^{3+} ions for the luminescent quenching[57]. The UV–Vis spectra of other metal ions in aqueous solution showed only slight overlap with the excitation spectrum of $Eu_{0.47}Tb_{0.53}$-CTP-COOH. Moreover, the fluorescence lifetime of $Eu_{0.47}Tb_{0.53}$-CTP-COOH before and after the addition of Fe^{3+} ion presented no obvious change, demonstrating that the luminescent quenching process belongs to a static mechanism, and there is no energy transfer within the $Eu_{0.47}Tb_{0.53}$-CTP-COOH-Fe^{3+} system (Supplementary Fig. 33).

VOC decoding in vapor. The outstanding sensing performance of the $Eu_{0.47}Tb_{0.53}$-CTP-COOH PVA film incorporated with different metal ions in aqueous solution inspired our enormous interest in sensing trace VOCs in the vapor state, especially for some carcinogenic and toxic VOCs. In order to test the sensitivity and response rate of the $Eu_{0.47}Tb_{0.53}$-CTP-COOH PVA film as a vapor sensor, a set-up was fabricated by placing a $Eu_{0.47}Tb_{0.53}$-
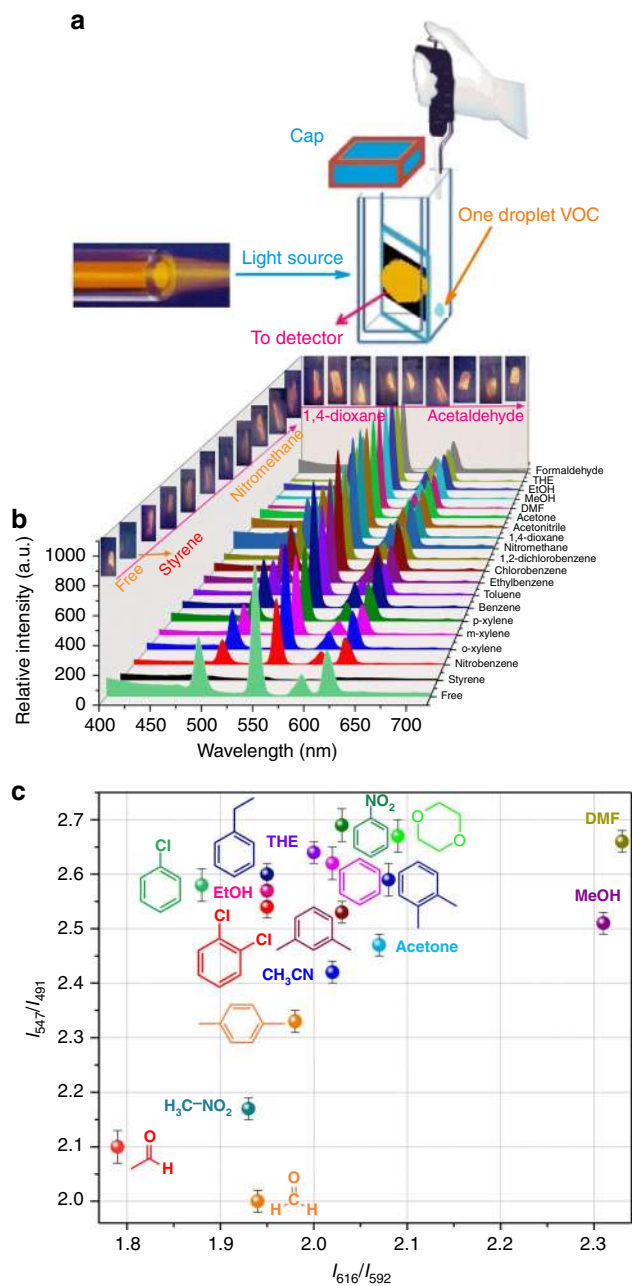
Fig. 5 VOC decoding in vapor. **a** In situ solid-state luminescent sensor set-up. **b** Emission spectra of $Eu_{0.47}Tb_{0.53}$-CTP-COOH PVA film exposed to different VOCs for 5 min. The inset shows the photographs of color changes for the sensor incorporated with different VOCs. **c** Two-dimensional decoded map of VOCs based on the emission intensity ratio (I_{616}/I_{592}) of Eu^{3+} ion as x-axis and the ratio (I_{547}/I_{491}) of Tb^{3+} as y-axis

CTP-COOH PVA film into a cell, followed by adding one droplet (ca. 5 μL) of VOCs (including styrene, nitrobenzene, o-xylene, m-xylene, p-xylene, benzene, toluene, ethylbenzene, chlorobenzene, 1,2-dichlorobenzene, nitromethane, 1,4-dioxane, acetonitrile, acetone, DMF, MeOH, ethanol, THF, formaldehyde, and acet-aldehyde) into the cell (Fig. 5a). The cell was then capped to form a hermetic environment, and the luminescent response of the $Eu_{0.47}Tb_{0.53}$-CTP-COOH PVA film for VOCs was recorded after 5 min. As shown in Fig. 5b, styrene exhibited a significant quenching effect on the characteristic emission of the $Eu_{0.47}Tb_{0.53}$-CTP-COOH PVA film, and the emission intensity at 547 nm for Tb^{3+} ion and 616 nm for Eu^{3+} was almost completely

quenched within 5 min. However, other VOCs only showed slight enhancement effect (DMF, MeOH, ethanol, acetone, acetonitrile, and acetaldehyde) or mild quenching effect (nitrobenzene) on the luminescence intensity of the $Eu_{0.47}Tb_{0.53}$-CTP-COOH PVA film (Fig. 5b and Supplementary Fig. 34). Therefore, styrene vapor could be effectively detected based on the $Eu_{0.47}Tb_{0.53}$-CTP-COOH PVA film as a sensor.

As compared with the sensing effect of the $Eu_{0.47}Tb_{0.53}$-CTP-COOH PVA film for metal ions, the characteristic emission intensity of Eu^{3+} or Tb^{3+} ion showed nonspecific enhancement or quenching to VOCs. However, these VOCs could still be easily distinguished based on characteristic emission intensity ratios of Tb^{3+} ion (I_{547}/I_{491}) and Eu^{3+} ion (I_{616}/I_{592}). These results clearly indicate that the $Eu_{0.47}Tb_{0.53}$-CTP-COOH PVA film is an excellent sensor for probing different VOCs. This kind of luminescent sensor for detecting different VOCs is remarkable, because it does not need any additional calibration. The interesting VOC-dependent emission of the $Eu_{0.47}Tb_{0.53}$-CTP-COOH PVA film can be ascribed to guest-dependent energy transfer from ligand CTP-COOH to Eu^{3+}/Tb^{3+} ions. Therefore, the characteristic emission intensity of the $Eu_{0.47}Tb_{0.53}$-CTP-COOH PVA film is relatively sensitive to the included VOCs by tuning the energy transfer from CTP-COOH to Eu^{3+}/Tb^{3+} ions. The emission intensity ratios of I_{547}/I_{491} for Tb^{3+} ion and I_{616}/I_{592} for Eu^{3+} ion is almost constant, and unique for each VOC guest in the luminescent spectrum of the $Eu_{0.47}Tb_{0.53}$-CTP-COOH PVA film. Such characteristic relationship between VOCs and the film sensor could be used to draw an emission-fingerprint map of VOCs based on the ratio of I_{616}/I_{592} as x-axis and the ratio of I_{547}/I_{491} as y-axis (Fig. 5c). This internal reference strategy is an excellent approach to solve the problem of variable emission intensity encountered when detecting VOCs by a single emissive transition. As shown in Fig. 5c, even for those VOCs having very similar structural motifs such as isomers of o-xylene, m-xylene, and p-xylene, as well as homologs of benzene, toluene, and ethylbenzene, they could still be unambiguously distinguishable.

Styrene sensing in vapor. As a potential human carcinogen, styrene vapor may be harmful to skin, eyes, and respiratory system. At high levels (10,000 ppm) of styrene vapor, rats and pigs become comatose after several minutes, even died after 30 to 60 min of exposure[58]. Therefore, it is necessary to develop con-venient and reliable sensors for the styrene detection. However, fluorescent sensors for styrene have not been fully developed until now.

The obtained results indicate that the $Eu_{0.47}Tb_{0.53}$-CTP-COOH PVA film is a promising candidate for the styrene detection. Supplementary Movies 1 and 2 show that yellow emission of the $Eu_{0.47}Tb_{0.53}$-CTP-COOH PVA film under UV 254 nm became faded gradually until completely disappeared in the styrene environment. As shown in Fig. 6a, time-dependent emission spectra of the $Eu_{0.47}Tb_{0.53}$-CTP-COOH PVA film in styrene vapor (ca. 5 μL) show remarkable quenching effect, i.e., >50% and 47% fluorescent quenching at 547 nm for Tb^{3+} ion and at 616 nm for Eu^{3+} ion within 1 min, respectively. When the response time was up to 4 min, the characteristic emission of Eu^{3+} and Tb^{3+} ions were almost completely quenched. Furthermore, time-dependent fluorescent decay curves of the $Eu_{0.47}Tb_{0.53}$-CTP-COOH PVA film at 547 and 616 nm upon the addition of styrene (ca. 5 μL) can be well fitted using single exponential functions (Fig. 6c, d), and the observed rate constants ($K_{obs} = 1/t_{1/2}$, $t_{1/2}$ is observed half-life) and $t_{1/2}$ are 0.0118 s^{-1}, 58.55 s for Tb^{3+} ion at 547 nm, and 0.0097 s^{-1}, 71.27 s for Eu^{3+} at 616 nm, respectively. These results (high K_{obs}, short $t_{1/2}$, and short response time) indicate that the response of the $Eu_{0.47}Tb_{0.53}$-CTP-COOH PVA
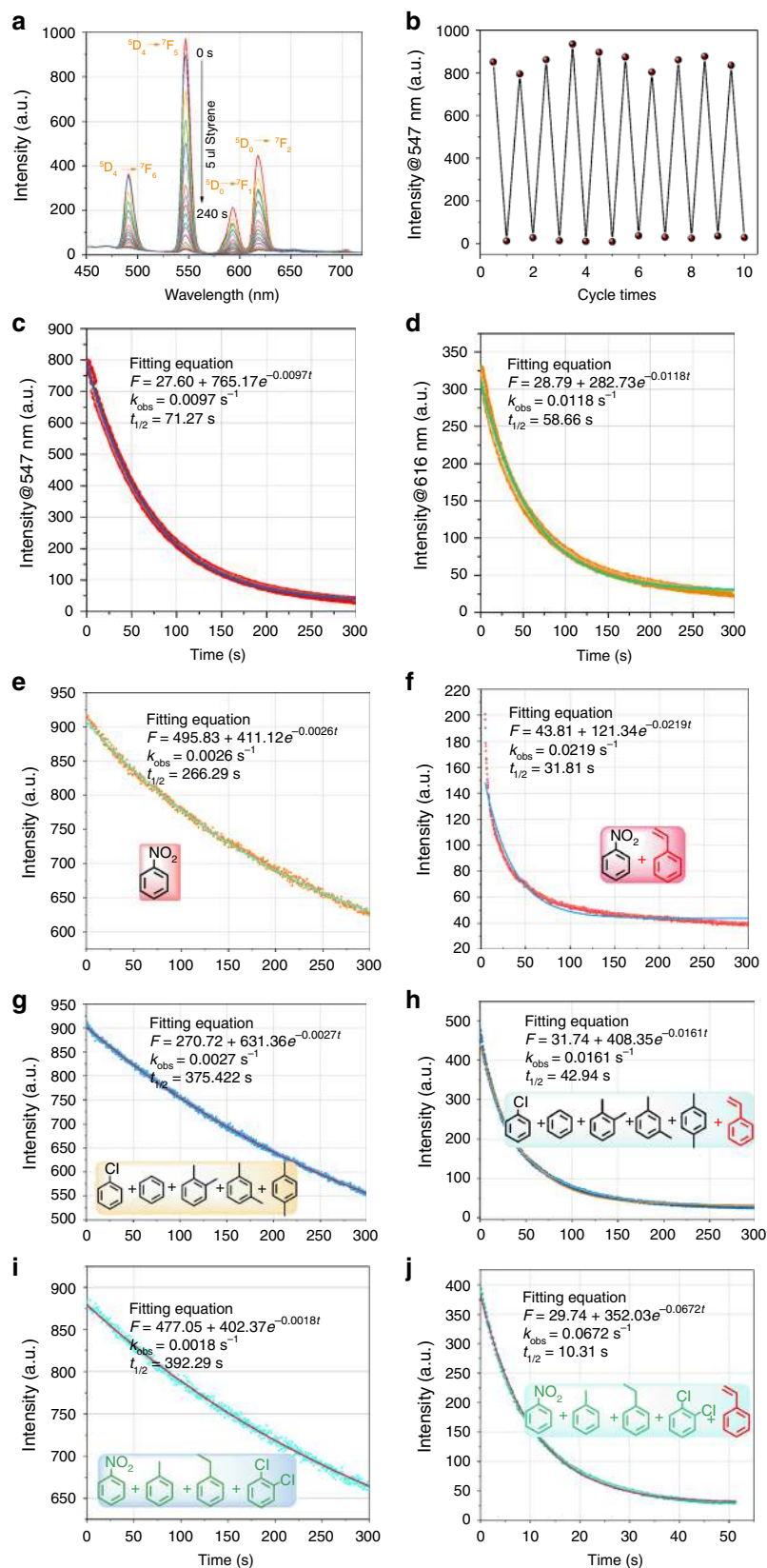
Fig. 6 Sensing properties of styrene in vapor. **a** Time-dependent luminescent spectra of the $Eu_{0.47}Tb_{0.53}$-CTP-COOH PVA film responded to 5 µL styrene vapor. **b** Quenching and recovery tests of the $Eu_{0.47}Tb_{0.53}$-CTP-COOH PVA film for styrene vapor. **c**, **d** Time-dependent fluorescent decay curves of the $Eu_{0.47}Tb_{0.53}$-CTP-COOH PVA film at 547 and 616 nm upon the addition of styrene vapor (2.27 mg/cm^3, 5 µL). **e–j** Time-dependent fluorescent decay curves of the $Eu_{0.47}Tb_{0.53}$-CTP-COOH PVA film at 547 nm and 616 nm in the presence of one or more interference VOCs
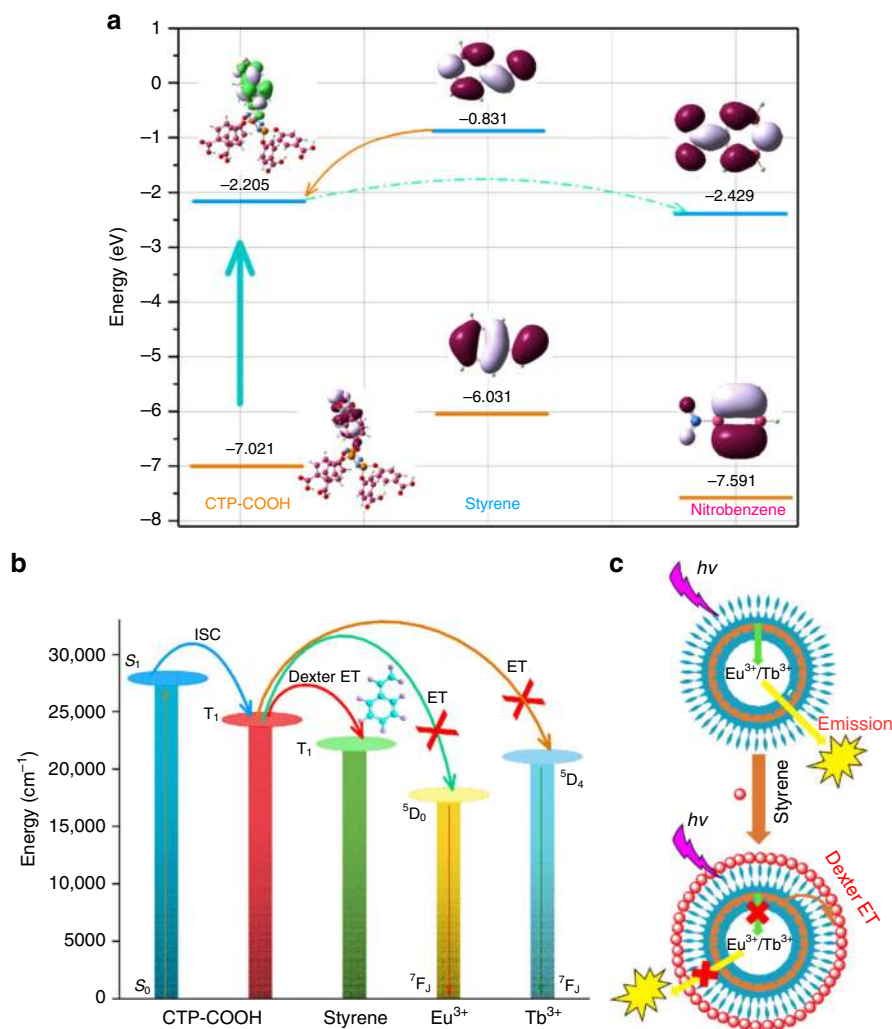
Fig. 7 Sensing mechanism of styrene. **a** Schematic representation of electronic structures of ligand CTP-COOH, styrene and nitrobenzene. **b** Simplified schematic diagram of LMET and Dexter-ET process in $Eu_{0.47}Tb_{0.53}$-CTP-COOH with styrene. **c** Schematic illustration of the mechanism of styrene sensing by $Eu_{0.47}Tb_{0.53}$-CTP-COOH

film for styrene vapor is extremely quick. In addition, the $Eu_{0.47}Tb_{0.53}$-CTP-COOH PVA film exhibits (Supplementary Figs. 35 and 36) similar response behavior in lower concentration environment of styrene vapor (2 μL). Single exponential fitted results of time-dependent fluorescent decay curves for the $Eu_{0.47}Tb_{0.53}$-CTP-COOH PVA film also present that this styrene sensor can effectively recognize and detect styrene molecule in the presence of other interference VOCs (Fig. 6e–j). For instance, the K_{obs} and $t_{1/2}$ values of the sensor in nitrobenzene vapor environment are $0.0026 \, s^{-1}$ and 266.29 s, respectively. But, higher K_{obs} ($0.0219 \, s^{-1}$) and shorter $t_{1/2}$ (31.81 s) were observed in the mixture environment of nitrobenzene and styrene vapors. Under more interference VOCs (nitrobenzene, toluene, ethylbenzene, and 1,2-dichlorobenzene), when inducing styrene into the sensing system, the value of K_{obs} increased from 0.0018 to $0.0672 \, s^{-1}$, i.e., 37 times of enhancement.

The repeatability for a sensory material is a crucial parameter to assess the sensor practicability. After the detection of styrene, the sample of $Eu_{0.47}Tb_{0.53}$-CTP-COOH PVA film@styrene could be recovered by simply heating at 100 °C for 3 h. The powder XRD pattern (Supplementary Fig. 37) of the recovered $Eu_{0.47}Tb_{0.53}$-CTP-COOH PVA film matched well with the as-prepared $Eu_{0.47}Tb_{0.53}$-CTP-COOH PVA film. As shown in Fig. 6b, the characteristic emission intensity at 547 nm after ten

cycles remained unchanged, and its powder XRD pattern still matched well with the as-prepared one (Supplementary Fig. 37), confirming its good stability and reusability.

Sensing mechanism of styrene. The mechanism for the detection of styrene by the $Eu_{0.47}Tb_{0.53}$-CTP-COOH PVA film was further investigated in detail. In this study, there are three reasons that can cause the fluorescence quenching of the $Eu_{0.47}Tb_{0.53}$-CTP-COOH PVA film in the presence of styrene vapor: (1) styrene induced framework collapse of the $Eu_{0.47}Tb_{0.53}$-CTP-COOH PVA film, (2) direct interaction of styrene with the emission centers of Ln^{3+}, and (3) styrene interaction with the ligand of the $Eu_{0.47}Tb_{0.53}$-CTP-COOH PVA film. As shown in Supplementary Figs. 38 and 39, the film sensor treated by styrene presents very similar powder XRD pattern to the original film sensor, indicating that the framework remains intact in the presence of styrene. Furthermore, styrene has no available functional groups to coordinate with Ln^{3+}, and thus has no direct interaction with Ln^{3+}. Therefore, the luminescence quenching of the $Eu_{0.47}Tb_{0.53}$-CTP-COOH PVA film under styrene is most likely due to the interaction between styrene and CTP-COOH ligand. The luminescence quenching is typically attributed to photoinduced electron transfer (PET), Förster resonance energy transfer (FRET), or Dexter electron transfer (ET) mechanism[59, 60]. In general, the

main driving force for PET is the energy gap between the lowest unoccupied molecular orbitals (LUMO) of donor and acceptor, and the donor should have higher energy level of LUMO than that of acceptor if PET is the luminescence quenching mechanism.[59, 61, 62] However, as calculated by the density functional theory (DFT) at the B3LYP/6-31 G* level (Fig. 7a), the LUMO energy level of the ligand CTP-COOH (donor) is obviously lower than that of styrene (acceptor). This result eliminates the possibility of the PET process on the luminescence quenching of the $Eu_{0.47}Tb_{0.53}$-CTP-COOH PVA film by styrene. In addition, the absorption spectrum of styrene has no obvious overlap with the emission spectrum of ligand CTP-COOH, and thus the FRET mechanism could also be ruled out. On the other hand, mild quenching effect of nitrobenzene for the fluorescence of the $Eu_{0.47}Tb_{0.53}$-CTP-COOH PVA film could be ascribed to the PET mechanism.

The emission lifetime of the $Eu_{0.47}Tb_{0.53}$-CTP-COOH PVA film in the absence and presence of styrene vapor is 0.47 and 0.38 ms, respectively (Supplementary Figs. 39 and 40), suggesting that the most possible quenching mechanism of styrene should be attributed to the Dexter-ET from triplet level (T_1) of ligand CTP-COOH to the triplet of styrene[63]. In this work, bright yellow emission of the $Eu_{0.47}Tb_{0.53}$-CTP-COOH PVA film is based on the ligand-to-metal energy transfer (LMET) process: the ligand strongly absorbs UV light, and then transfers the absorbed energy to $^5D_0$ level of Eu^{3+} ion and $^5D_4$ level of Tb^{3+} ion, thus promoting the characteristic emission of Eu^{3+} and Tb^{3+} ions (Fig. 7). In the presence of styrene, since the calculated triplet energy level (T_1) of styrene lies between triplet T_1 of ligand CTP-COOH and $^5D_0$ level of Eu^{3+}, the ligand CTP-COOH and styrene compete with the LMET process through suppressing or blocking the energy transfer from the ligand to Ln^{3+} ions. As a result, the emission of the $Eu_{0.47}Tb_{0.53}$-CTP-COOH PVA film is restricted or quenched, and thus styrene is successfully detected (Fig. 7b, c).

Discussion

In summary, we have developed a new strategy using bimetallic Eu^{3+}/Tb^{3+} MOFs as self-calibrating luminescent sensors for distinguishing different metal ions in aqueous solution and VOCs in vapor. The bimetallic Ln-MOFs serve as a luminescent platform owing to excellent fingerprint correlation between metal ions/VOCs and characteristic emission intensity ratios of I_{547}/I_{491} for Tb^{3+} ion and I_{616}/I_{592} for Eu^{3+} ion. We have successfully demonstrated the first decoded map that can effectively and reliably distinguish different metal ions in aqueous solution based on the emission intensity ratios of I_{616}/I_{592} for Eu^{3+} ion as the x-axis and $I_{547}I_{491}$ for Tb^{3+} ion as the y-axis. According to this decoded map, different metal ions in aqueous solution could be easily recognized. Based on a similar principle, a decoded map for sensing different VOCs in vapor has also been established. Such versatile bimetallic Ln-MOF sensor exhibits high sensitivity and selectivity for Fe^{3+} ion in aqueous solution and styrene in vapor. The capability to unambiguously recognize metal ions/VOCs makes bimetallic Ln-MOFs a promising luminescent platform with potentially valuable applications.

Methods

Materials and methods. All reagents and chemicals were purchased commercially (Sigma-Aldrich and Alfa) and used without further purifications unless otherwise specified. FT-IR spectra were carried out using a Nicolet Is-10 (Nicolet) Fourier Transform Infrared Spectrometer. TGA was made with TA Q50 at a heating rate of 15 °C/min under N_2 atmosphere and over a temperature range from room temperature to 800 °C. All the ESI-MS spectra were recorded in LCQ DECA XP mass spectrometer. NMR spectra were taken on a DRX-400 MHz (Bruker) superconducting-magnet NMR spectrometer with TMS as an internal standard. UV–Vis absorption spectrum was determined on a Shimadzu UV-3600

UV–Vis–NIR spectrophotometer. The photoluminescence measurements in the solid state and THF solution were conducted in a Shimadzu RF-5301PC fluorescence spectrophotometer. Fluorescent lifetimes were obtained with the FLS980 steady state spectrometer with a pulsed xenon lamp. ICP-MS data were obtained on an ICP-9000 ($N + M$) inductively coupled plasma emission spectrometer. Scanning electron microscope images were performed on a JSM-6700F (JEOL) equipped with an energy-dispersive X-ray spectroscopy (EDS) instrument. Powder XRD measurements were recorded on a Rigaku D/Max-2500 X-ray diffractometer using Cu Kα radiation with 2θ range of 2–50°, 40 KeV, and 30 mA having a scanning rate of 0.01° s^{-1} (2θ) at room temperature.

Synthesis of methyl 4-hydroxybenzoate. 4-Hydroxy benzoic acid (35 mmol, 5.3 g) and MeOH (80 mL) were taken in a 150 mL round-bottom flask fitted with a reflux condenser. Concentrated sulfuric acid (2.5 mL) was added as a catalyst and the contents were refluxed for 12 h. The reaction mixture was cooled and excess MeOH was removed using a rotary evaporator. The residue obtained was dissolved in chloroform and washed thoroughly with 10% sodium bicarbonate solution. The organic layer was dried over anhydrous $MgSO_4$ and concentrated to give the product in 95% yield. ^1H NMR (400 Hz, CDCl$_3$, ppm): 7.973–7.951 (d, 2 H, Ar–H), 6.887–6.865 (d, 2 H, Ar–OH), 5.8 (s, 1 H, Ar–OH), 3.896 (s, 3 H, COOCH$_3$).

Synthesis of hexa-(4-carbomethoxy-phenoxy)-cyclotriphosphazene (CTP-COOCH$_3$). Potassium carbonate (11.38 g, 0.082 mol) and methyl 4-hydroxybenzoate (6.54 g, 0.043 mol) were added into a 250 mL round-bottom flask, and then methyl 4-hydroxybenzoate was dissolved by dry THF (120 mL). The mixture solution was heated to 70 °C under the N_2, and $P_3N_3Cl_6$ (2.49 g, 0.007 mol) was added. The mixture was stirred at this temperature overnight. The solvent was removed by evaporation under a reduced pressure, and the obtained solid was redissolved in dichloromethane (70 mL). The organic phase was washed with deionized water and then dried over anhydrous $MgSO_4$. Dichloromethane was removed by evaporation under a reduced pressure, the white powder was heated at 60 °C by vacuum oven overnight, and the desired product was obtained (6.1 g, yield 83.7%). ^1H NMR (400 MHz, DMSO-d_6, ppm): 7.77–7.79 (d, 12 H, Ar–H), 7.03–7.06 (d, 12 H, Ar–H), 3.87 (s, 18 H, –COOCH$_3$). ^{13}C NMR (CDCl$_3$, 100 MHz, ppm):165.98, 153.62, 131.35, 127.36, 120.57, 52.30.

Synthesis of ligand hexa-(4-carboxyl-phenoxy)-cyclotriphosphazene (CTP-COOH). Sodium hydroxide (1.8 g, 45 mmol) was dissolved in deionized water (80 mL), CTP-COOCH$_3$ (5 g, 4.8 mmol) was dissolved by THF (100 mL), and two solutions were mixed. The mixture was stirred for 1.5 h at 70 °C. After the reaction, THF was removed by rotatory evaporator, and the residual solution was poured into deionized water (300 mL) with dilute hydrochloric acid acidified to pH ca. 2–3. The product as a precipitate was obtained after stirring. The precipitate was collected by filtration, washed with deionized water and dried at 60 °C overnight by vacuum oven. The desired ligand CTP-COOH was obtained as white powder (4.3 g, yield 94%). FT-IR (KBr): v/cm^{-1} 3002.38, 2668.64, 2538.03, 1697.86, 1602.81, 1507.77, 1281.41, 1150.08, 947.66, 774.98, 548.61. ^1H NMR (400 MHz, DMSO-d_6, ppm) 13.05 (s, 6 H, –COOH), 7.86–7.84 (d, 12 H, Ar–H), 7.00–7.03 (d, 12 H, Ar–H). ^{13}C NMR (300 MHz, DMSO-d_6, ppm) 166.69, 153.23, 131.82, 128.82. ESI-MS: 980.09 (CTP-COOH + Na$^+$).

Typical synthesis of [Eu$_x$Tb$_{1-x}$-CTP-COOH·(H$_2$O)$_3$] (x = 1, 0.84, 0.69, 0.47, 0.38, 0.19, 0.12, 0.06, 0). These Eu/Tb-MOFs were synthesized according to the following procedure[3]. According to the pre-designed ratio, Eu$_x$Tb$_y$Cl$_3$•H$_2$O ($x + y$ = 0.5 mmol) and ligand (0.5 mmol) were placed in a 50 mL vial. Deionized water (6 mL) and NaOH solution (0.5 mL, 2 M) were added, and the mixture was stirred at room temperature. After 10 min, warm cyclohexanol (7 mL) was added and the biphasic mixture was stirred for 15 min. The vial was heated to 100 °C and kept at this temperature for 5 days. The colorless crystal was obtained after washing several times with ethanol. The Eu^{3+}/Tb^{3+} ratio in reaction as well as the lanthanide concentration in the final product is listed in Supplementary Table 1.

Preparation of luminescent platform. The luminescent platform $Eu_{0.47}Tb_{0.53}$-CTP-COOH PVA film was prepared as follows. First, PVA (1 g, Mw 85,000–124,000, 99 + % hydrolyzed) was dissolved in deionized water (100 mL) at 85 °C for 1.5 h to afford PVA solution (10 g/L). Next, the ground $Eu_{0.47}Tb_{0.53}$-CTP-COOH powder (10 mg) was dispersed in PVA solution (10 mL), and the sample was treated under ultrasonicaton for 0.5 h to achieve uniformly dispersed $Eu_{0.47}Tb_{0.53}$-CTP-COOH PVA suspension (Ln-MOF concentration: 1 mg/mL). Finally, dropping the $Eu_{0.47}Tb_{0.53}$-CTP-COOH PVA suspension onto the polyethylene glycol terephthalate sheet (1 × 2.5 cm) and drying at 60 °C for 3 h afforded the desired luminescent platform.

X-ray crystal structure determination. Diffraction intensity data for single crystal of Ln-MOFs Eu-CTP-COOH (Supplementary Data 1) and Tb-CTP-COOH (Supplementary Data 2) were collected at 100 K on a Bruker Apex II CCD diffractometer equipped with graphite-monochromated Mo-Kα radiation (λ = 0.71073 Å). Data processing was accomplished with the Bruker SAINT software

package. Absorption corrections were applied using the Numerical Mu from Formula method (SADABS). The structure was solved by direct methods using SHELXS-97 program of the SHELXTL package and refined by using the full-matrix least squares method on F^2 with SHELXTL-97. Anisotropic displacement parameters were applied to all non-hydrogen atoms. Hydrogen atoms were located geometrically and were added to the structure factor calculation.

Quantum yield (Φ) measurements. The quantum yield (Φ) was determined by employing the method reported in literature[64], and Φ of a given material could be calculated by a direct comparison with standard phosphors having known Φ values. The quantum yield could be calculated from the following equation:

$$\Phi = \frac{1 - R_x}{1 - R_{ST}} \times \frac{I_{ST}}{I_x} \times \Phi s_{ST} \qquad (1)$$

where R_{ST} and R_x apply for these exciting radiation reflected by the standard and the sample, respectively, and Φ_{ST} is the quantum yield of the standard phosphor. The I_{ST} and I_x terms correspond to the integrated photon flux (photon s^{-1}) for the sample and standard phosphors. Sodium salicylate was chosen as the standard and the Φ_{ST} reported is 55% at room temperature[65].

Metal ion decoding and Fe^{3+} ion sensing in aqueous solution. Decoding metal ions: The luminescent platform $Eu_{0.47}Tb_{0.53}$-CTP-COOH PVA film was immersed into different metal ions (1×10^{-2} M) for 30 min, then the emission spectra of $Eu_{0.47}Tb_{0.53}$-CTP-COOH PVA film@Metal ions were recorded ($\lambda_{ex} = 280$ nm, slit: 5 nm).

Sensing for Fe^{3+} ion: The $Eu_{0.47}Tb_{0.53}$-CTP-COOH PVA film was immersed in deionized water in a quartz cell (2 mL). Then, the Fe^{3+} aqueous solution was gradually added by a micro syringe, and luminescent spectra were recorded after 3 min equilibration.

VOC decoding and styrene probing in vapors. Decoding VOCs: A home-made set-up was fabricated by placing a $Eu_{0.47}Tb_{0.53}$-CTP-COOH PVA film into the cell, followed by adding one drop (5 μL) of VOCs (styrene, nitrobenzene, o-xylene, m-xylene, p-xylene, benzene, toluene, ethylbenzene, chlorobenzene, 1,2-dichlorobenzene, nitromethane, 1,4-dioxane, acetonitrile, acetone, DMF, MeOH, ethanol, THF, formaldehyde, and acetaldehyde) into the cell. The cell was then capped to form a hermetic environment, and then luminescent response of $Eu_{0.47}Tb_{0.53}$-CTP-COOH PVA film towards VOCs was recorded after 5 min.

Probing for styrene in vapors: The luminescent platform $Eu_{0.47}Tb_{0.53}$-CTP-COOH PVA film was fixed into the cell, followed by adding one droplet styrene (2 μL OR 5 μL) into the cell. The cell was then capped, and time-dependent luminescent spectra were recorded.

References
1. Carter, K. P., Young, A. M. & Palmer, A. E. Fluorescent sensors for measuring metal ions in living systems. *Chem. Rev.* **114**, 4564–4601 (2014).
2. Song, X. Z. et al. Single-crystal-to-single-crystal transformation of a europium (III) metal-organic framework producing a multi-responsive luminescent sensor. *Adv. Funct. Mater.* **24**, 4034–4041 (2014).
3. Shenashen, M. A., El-Safty, S. A. & Elshehy, E. A. Architecture of optical sensor for recognition of multiple toxic metal ions from water. *J. Hazard. Mater.* **260**, 833–843 (2013).
4. Hwang, K. et al. Photocaged DNAzymes as a general method for sensing metal ions in living cells. *Angew. Chem. Int. Ed.* **53**, 13798–13802 (2014).
5. Ding, S. Y. et al. Thioether-based fluorescent covalent organic framework for selective detection and facile removal of mercury(II). *J. Am. Chem. Soc.* **138**, 3031–3037 (2016).
6. Weishaupt, R. et al. A protein-nanocellulose paper for sensing copper ions at the nano- to micromolar level. *Adv. Funct. Mater.* **27**, 1604291 (2017).
7. Yang, G. H., Wan, X. J., Su, Y. K., Zeng, X. R. & Tang, J. N. Acidophilic S-doped carbon quantum dots derived from cellulose fibers and their fluorescence sensing performance for metal ions in an extremely strong acid environment. *J. Mater. Chem. A* **4**, 12841–12849 (2016).
8. Hoang, M., Huang, P. J. & Liu, J. W. G-Quadruplex DNA for fluorescent and colorimetric detection of thallium(I). *ACS Sens.* **1**, 137–143 (2016).
9. Dang, S., Ma, E., Sun, Z. M. & Zhang, H. A layer-structured Eu-MOF as a highly selective fluorescent probe for Fe^{3+} detection through a cation-exchange approach. *J. Mater. Chem.* **22**, 16920–16926 (2012).
10. Zheng, M. et al. Fast response and high sensitivity europium metal organic framework fluorescent probe with chelating terpyridine sites for Fe^{3+}. *ACS Appl. Mater. Interfaces* **5**, 1078–1083 (2013).
11. Chen, D. M., Zhang, N. N., Liu, C. S. & Du, M. Template-directed synthesis of a luminescent Tb-MOF material for highly selective Fe^{3+} and Al^{3+} ion detection and VOC vapor sensing. *J. Mater. Chem. C.* **5**, 2311–2317 (2017).
12. Xu, H., Hu, H. C., Cao, C. S. & Zhao, B. Lanthanide organic framework as a regenerable luminescent probe for Fe^{3+}. *Inorg. Chem.* **54**, 4585–4587 (2015).
13. Bai, G. X., Tsang, M. K. & Hao, J. H. Luminescent ions in advanced composite materials for multifunctional applications. *Adv. Funct. Mater.* **26**, 6330–6350 (2016).
14. Adinarayana, B., Thomas, A. P., Yadav, P., Kumar, A. & Srinivasan, A. Bipyricorrole: a corrole homologue with a monoanionic core as a fluorescence Zn^{II} sensor. *Angew. Chem. Int. Ed.* **55**, 969–973 (2016).
15. Li, Y. T. et al. Core–shell upconversion nanoparticle@metal–organic framework nanoprobes for luminescent/magnetic dual-mode targeted imaging. *Adv. Mater.* **27**, 4075–4080 (2015).
16. Hosomi, T., Masai, H., Fujihara, T., Tsuji, Y. & Terao, J. A typical metal-ion-responsive color-tunable emitting insulated π-conjugated polymer film. *Angew. Chem. Int. Ed.* **55**, 13427–13431 (2016).
17. Li, H., Zhang, P., Smaga, L. P., Hoffman, R. A. & Chan, J. Photoacoustic probes for ratiometric imaging of copper(II). *J. Am. Chem. Soc.* **137**, 15628–15631 (2015).
18. Beer, P. D. & Gale, P. A. Anion recognition and sensing: the state of the art and future perspectives. *Angew. Chem. Int. Ed.* **40**, 486–516 (2001).
19. Li, Y. T. et al. Coordination-responsive drug release inside gold nanorod@metal-organic framework core–shell nanostructures for near-infrared-induced synergistic chemo-photothermal therapy. *Nano Res.* https://doi.org/10.1007/s12274-017-1874-y (2017).
20. He, L. C. et al. Core–shell noble-metal@metal-organic-framework nanoparticles with highly selective sensing property. *Angew. Chem. Int. Ed.* **52**, 3741–3745 (2013).
21. Zhou, Y. & Yan, B. A responsive MOF nanocomposite for decoding volatile organic compounds. *Chem. Commun.* **52**, 2265–2268 (2016).
22. Liu, Y. L. & Tang, Z. Y. Multifunctional nanoparticle@MOF core–shell nanostructures. *Adv. Mater.* **25**, 5819–5825 (2013).
23. Dong, M. J., Zhao, M., Ou, S., Zou, C. & Wu, C. D. A luminescent dye@MOF platform: emission fingerprint relationships of volatile organic molecules. *Angew. Chem. Int. Ed.* **53**, 1575–1579 (2014).
24. Yang, X. L. et al. A multiresponsive metal–organic framework: direct chemiluminescence, photoluminescence, and dual tunable sensing applications. *Adv. Funct. Mater.* **26**, 393–398 (2016).
25. Small, L. J. & Neno, T. M. Direct electrical detection of iodine gas by a novel metal-organic-framework-based sensor. *ACS Appl. Mater. Interfaces* **9**, 44649–44655 (2017).
26. Zhou, Z. C. et al. Internanofiber spacing adjustment in the bundled nanofibers for sensitive fluorescence detection of volatile organic compounds. *Anal. Chem.* **89**, 3814–3818 (2017).
27. Wang, Y. et al. Real-time detection of styrene using SAW sensors based on hexafluoroisopropanol group functionalized hydrogen-bond acidic polymers. *Sens. Actuators B* **206**, 252–257 (2015).
28. Van Rooij, J. G. M. et al. Trends in occupational exposure to styrene in the European glass fibre-reinforced plastics industry. *Ann. Occup. Hyg.* **52**, 337–349 (2008).
29. Babaee, R., Bonakdarpour, B., Nasernejad, B. & Fallah, N. Kinetics of styrene biodegradation in synthetic wastewaters using an industrial activated sludge. *J. Hazard. Mater.* **184**, 111–117 (2010).
30. Johnson, A. C. Relationship between styrene exposure and hearing loss: review of human studies. *Int. J. Occup. Med. Environ. Health* **20**, 15–325 (2007).
31. Lawton, B. W., Hoffmann, J. & Triebig, G. The ototoxicity of styrene: a review of occupational investigations. *Int. Arch. Occup. Environ. Health* **79**, 93–102 (2006).
32. Rueff, J., Teixeira, J. P. L., Santos, S. & Gaspar, J. F. Genetic effects and biotoxicity monitoring of occupational styrene exposure. *Clin. Chim. Acta* **399**, 8–23 (2009).
33. Prado, C., Ibarra, I. & Periago, J. F. Evaluation of styrene in air by thermal desorption-gas chromatography. *J. Chromatogr. A* **778**, 255–262 (1997).
34. Chen, Q. F., Milburn, R. K. & Karellas, N. S. Real time monitoring of hazardous airborne chemicals: a styrene investigation. *J. Hazard. Mater.* **132**, 261–268 (2006).
35. Cui, Y. J. et al. A luminescent mixed-lanthanide metal-organic framework thermometer. *J. Am. Chem. Soc.* **134**, 3979–3982 (2012).

36. Sava, D. F., Rohwer, L. E. S., Rodriguez, M. A. & Nenoff, T. M. Intrinsic broad-band white-light emission by a tuned, corrugated metal−organic framework. *J. Am. Chem. Soc.* **134**, 3983–3986 (2012).

37. Sava, D. F., Rohwer, L. E. S., Rodriguez, M. A. & Nenoff, T. M. Efficient photoluminescence via metal—ligand alteration in a new MOFs family. *Chem. Mater.* **26**, 2943–2951 (2014).

38. Sava, D. F. et al. Multifunctional, tunable metal–organic framework materials platform for bioimaging applications. *ACS Appl. Mater. Interfaces* **9**, 22268–22277 (2017).

39. Betard, A. & Fischer, R. A. Metal-organic framework thin films: from fundamentals to applications. *Chem. Rev.* **112**, 1055–1083 (2012).

40. Achmann, S. et al. Metal-organic frameworks for sensing applications in the gas phase. *Sensors* **9**, 1574–1589 (2009).

41. Li, L. et al. Visible-light excited luminescent thermometer based on single lanthanide organic frameworks. *Adv. Funct. Mater.* **26**, 8677–8684 (2016).

42. Cui, Y. et al. Dual-emitting MOF ⊃ dye composite for ratiometric temperature sensing. *Adv. Mater.* **27**, 1420–1425 (2015).

43. Hao, J. N. & Yan, B. Amino-decorated lanthanide(III) organic extended frameworks for multi-color luminescence and fluorescence sensing. *J. Mater. Chem. C.* **2**, 6758–6764 (2014).

44. Asha, K. S., Bhattacharjee, R. & Mandal, S. Complete transmetalation in a metal–organic framework by metal ion metathesis in a single crystal for selective sensing of phosphate ions in aqueous media. *Angew. Chem. Int. Ed.* **55**, 11528–11532 (2016).

45. Gai, Y. L. et al. Mixed-lanthanide metal–organic frameworks with tunable color and white light emission. *Cryst. Growth Des.* **17**, 940–944 (2017).

46. Feng, R. et al. Novel luminescent three-dimensional heterometallic complexes with 2-fold interpenetrating (3,6)-connected nets. *Cryst. Growth Des.* **11**, 1705–1712 (2011).

47. Li, B. et al. Temperature-controlled synthesis and luminescent properties of two novel coordination polymers modeled by hexa-carboxylate ligand derived from cyclotriphosphazene. *Dalton Trans.* **42**, 2588–2593 (2013).

48. Yu, W. J. et al. Lanthanide coordination polymers with hexa-carboxylate ligands derived from cyclotriphosphazene as bridging linkers: synthesis, thermal and luminescent properties. *CrystEngComm* **15**, 7732–7739 (2013).

49. Zhou, J. M. et al. A bimetallic lanthanide metal–organic material as a self-calibrating color-gradient luminescent sensor. *Adv. Mater.* **27**, 7072–7077 (2015).

50. Zhan, C., Ou, S., Zou, C., Zhao, M. & Wu, C. D. A luminescent mixed-lanthanide-organic framework sensor for decoding different volatile organic molecules. *Anal. Chem.* **86**, 6648–6653 (2014).

51. Zhou, Y., Chen, H. H. & Yan, B. An Eu^{3+} post-functionalized nanosized metal–organic framework for cation exchange-based Fe^{3+}-sensing in an aqueous environment. *J. Mater. Chem. A* **2**, 13691–13697 (2014).

52. Xiang, Z., Fang, C., Leng, S. & Cao, D. An amino group functionalized metal–organic framework as a luminescent probe for highly selective sensing of Fe^{3+} ions. *J. Mater. Chem. A* **2**, 7662–7665 (2014).

53. Xu, X. Y. & Yan, B. Eu(III)-functionalized MIL-124 as fluorescent probe for highly selectively sensing ions and organic small molecules especially for Fe (III) and Fe(II). *ACS Appl. Mater. Interfaces* **7**, 721–729 (2015).

54. Hou, G. G., Liu, Y., Liu, Q. K., Ma, J. P. & Dong, Y. B. NbO lattice MOFs based on octahedral M(II) and ditopic pyridyl substituted diketonate ligands: structure, encapsulation and guest-driven luminescent property. *Chem. Commun.* **47**, 10731–10733 (2011).

55. Zhou, J. M., Shi, W., Li, H. M., Li, H. & Cheng, P. Experimental studies and mechanism analysis of high-sensitivity luminescent sensing of pollutional small molecules and ions in Ln_4O_4 cluster based microporous metal–organic frameworks. *J. Phys. Chem. C.* **118**, 416–426 (2014).

56. Cheung, W. et al. π-Plasmon absorption of carbon nanotubes for the selective and sensitive detection of Fe^{3+} ions. *Chem. Sci.* **7**, 5192–5199 (2016).

57. Li, H., Wang, H. & Wang, L. Synthesis and sensing application of highly luminescent and water stable polyaspartate functionalized LaF_3 nanocrystals. *J. Mater. Chem. C.* **1**, 1105–1110 (2013).

58. Bearman, K. R. et al. A novel piezo-optical styrene sensor incorporating polymer-supported tribromide ion. *Chem. Commun.* 980–981 (2002).

59. Nagarkar, S. S., Joarder, B., Chaudhari, A. K., Mukherjee, S. & Ghosh, S. K. Highly selective detection of nitro explosives by a luminescent metal–organic framework. *Angew. Chem. Int. Ed.* **52**, 2881–2885 (2013).

60. Ramachandra, S. et al. Förster resonance energy transfer in quantum dot-dye-loaded zeolite L nanoassemblies. *Small* **7**, 1488–1494 (2011).

61. Germain, M. E. & Knapp, M. J. Optical explosives detection: from color changes to fluorescence turn-on. *Chem. Soc. Rev.* **38**, 2543–2555 (2009).

62. Xu, B. W., Wu, X. F., Li, H. B., Tong, H. & Wang, L. X. Selective detection of TNT and picric acid by conjugated polymer film sensors with donor–acceptor architecture. *Macromolecules* **44**, 5089–5092 (2011).

63. Qi, Z. W., You, Q. & Chen, Y. Nucleotide/Tb^{3+} coordination polymer nanoparticles as luminescent sensor and scavenger for nitrite ion. *Anal. Chim. Acta* **902**, 168–173 (2016).

64. Bril, A. & Jagerveenis, A. W. D. Some methods of luminescence efficiency measurements. *J. Res. Natl. Bur. Stand. Sect. A-Phys. Chem.* **80**, 401–407 (1976).

65. Malta, O. L. et al. Experimental and theoretical emission quantum yield in the compound Eu(thenoyltrifluoroacetonate)$_3$·2(dibenzyl sulfoxide). *Chem. Phys. Lett.* **282**, 233–238 (1998).

Acknowledgements

Author contributions

Y.S., J.H.Y., C.L.Y., C.D., and Y.L.Z.: conceived the project. Y.S., J.H.Y., and C.L.Y.: designed and performed most of experiments. Y.S., X.Z.Y., Y.B.L., C.L.Y., and Y.L.Z.: analysis of the data. R.G., S.Z.F.P., W.Q.L., and G.F.L.: performed the single crystal, FT-IR, TGA, and XRD experiments. Y.S. and C.L.Y.: carried out the syntheses. Y.S. and C.L. Y.: prepared the manuscript. S.Z.F.P., J.H.Y., W.Q.L., C.D., and Y.L.Z.: revised the manuscript. All the authors discussed the results and commented on the manuscript. Y.S. and J.H.Y. contributed equally to this work. C.D., C.L.Y., and Y.L.Z. supervised the project.

Additional information

Competing interests: The authors declare no competing interests.

Reprints and permission information is available online at http://npg.nature.com/reprintsandpermissions/

Publisher's note: Springer Nature remains neutral with regard to jurisdictional claims in published maps and institutional affiliations.